Author Manuscript

Author Manuscript

Author Manuscript

Author Manuscript

HHS Public Access

Author manuscript

J Biomol NMR. Author manuscript; available in PMC 2017 December 01.

Published in final edited form as:

J Biomol NMR. 2016 December ; 66(4): 259–271. doi:10.1007/s10858-016-0074-5.

^{15}N and ^{13}C-SOFAST-HMQC editing enhances 3D-NOESY sensitivity in highly deuterated, selectively [^{1}H,^{13}C]-labeled proteins

Paolo Rossi[*,†], **Youlin Xia**[†], **Nandish Khanra**, **Gianluigi Veglia**[*], and **Charalampos G. Kalodimos**[*]

Department of Biochemistry, Molecular Biology and Biophysics, University of Minnesota, Minneapolis, MN 55455

Abstract

The ongoing NMR method development effort strives for high quality multidimensional data with reduced collection time. Here, we apply 'SOFAST-HMQC' to frequency editing in 3D HMQC-NOESY-HMQC and demonstrate the sensitivity benefits using highly deuterated and ^{15}N, methyl labeled samples in H_2O. The experiments benefit from a combination of selective T_1 relaxation (or L-optimized effect), from Ernst angle optimization and, in certain types of experiments, from using the mixing time for both NOE buildup and magnetization recovery. This effect enhances sensitivity by up to 2.4× at fast pulsing versus reference HMQC sequences of same overall length and water suppression characteristics. Representative experiments designed to address interesting protein NMR challenges are detailed. Editing capabilities are exploited with heteronuclear ^{15}N,^{13}C-edited, or with diagonal-free ^{13}C aromatic/methyl-resolved 3D-SOFAST-HMQC-NOESY-HMQC. The latter experiment is used here to elucidate the methyl-aromatic NOE network in the hydrophobic core of the 19kDa FliT-FliJ flagellar protein complex. Incorporation of fast pulsing to reference experiments such as 3D-NOESY-HMQC boosts digital resolution, simplifies the process of NOE assignment and helps to automate protein structure determination.

Keywords

NOESY; SOFAST; SOFAST-NOESY; fast pulsing data collection; liquid state NMR

INTRODUCTION

Multidimensional NMR is a proven tool for studying protein structure and dynamics in the native state. (Gelis et al. 2007; Sprangers and Kay 2007) NMR-based structural biology efforts rely on nuclear Overhauser effect spectroscopy (NOESY) for structure elucidation and modeling to gain insights about the system function. Three dimensional ^{15}N,^{13}C-edited HMQC-NOESY-HMQC (Kay et al. 1990; Vuister et al. 1993; Zwahlen et al. 1998)

[*]Corresponding authors. rossip@umn.edu; vegli001@umn.edu; ckalodim@umn.edu.
[†]Authors that contributed equally to this work.

No competing financial interests have been declared.

Pulse sequences are freely available upon request from the corresponding authors.

Author Manuscript Author Manuscript Author Manuscript Author Manuscript

experiments are used routinely in the study of intermediate size proteins (~50 kDa) produced with labeled ^{2}H, ^{15}N and [^{1}H,^{13}C] on methyl groups. (Tugarinov et al. 2003) The methyl resonance assignment is conducted using a combination of methyl to backbone correlation and 3,4D-NOESY-HMQCs experiments. The simple HMQC editing scheme is ideally suited to leverage the methyl-TROSY effect in methyl labeled samples.

Fast pulsing techniques for rapid NMR data collection known as SOFAST-HMQC (Schanda et al. 2005) have garnered interest by making 2D ^{13}C and ^{15}N correlation spectroscopy possible within a few seconds in proteins and nucleic acids. (Amero et al. 2009; Sathyamoorthy et al. 2014) The SOFAST experiment has been applied to kinetic (Theillet et al. 2013), diffusion (Augustyniak et al. 2011), structural heterogeneity studies (Schanda et al. 2006a; Solyom et al. 2013), and 3D triple resonance experiments (Schanda et al. 2006b).

In this manuscript, we describe a series of heteronuclear NOESY experiments that combine 2D SOFAST-HMQC and NOESY with the goal of maximizing sensitivity and data quality. The experiments are intended for use with deuterated with U-^{15}N and selectively [^{1}H,^{13}C]-methyl and(or) aromatic labeled proteins. In such samples, the amide, methyl and aromatic moieties appear at distinct regions of the spectrum and are poised for selective excitation/observation. The experiments are based on the ^{15}N and ^{13}C-resolved versions of the 3D-HMQC-NOESY-HMQC, also known as the methyl NOESY, and 3D NOESY-HMQC.

We describe in detail several variations on the 3D SOFAST HMQC-NOESY-HMQC and 3D SOFAST NOESY-HMQC experiments, compare their sensitivity to that of the reference HMQC sequences and show that significant sensitivity and resolution improvements can be obtained. In order to support our findings, we conduct direct measurements of the selective T_1 recovery (L-optimized effect) (Pervushin et al. 2002) in our MBP ^{15}N methyl labeled sample, illustrate the theory basis for the experiment, compare the sensitivity and NOE buildup results of SOFAST and traditional NOESY. In addition, we characterize the contribution of the Ernst angle, its correct positioning in the sequence and its role in enhancing the NOE signal during fast pulsing. Depending on the experiment in question, distinct mechanisms are responsible for sensitivity enhancement, a significant effect is due to the additional recovery allowed during mixing time. At fast pulsing regime (0.2 s interscan delay) and ~0.3 s mixing that results into a doubling of the recovery time for the same overall acquisition time. As proof of principle, we demonstrate acquisition of four fully sampled methyl-amide 3D NOESYs in under one day on maltose binding protein (MBP, 42.5 kDa). Further applications and benefits of the experiments will be discussed.

MATERIALS AND METHODS

Production of methyl-aromatic labeled protein samples

A 1 mM *U*-[^{13}C,^{15}N] FliT$^{\Delta\alpha4}$-FliJ$^{51–101}$ and 1 mM *U*-[^{2}H,^{15}N] and Ala-$^{13}CH_3$, Met-$^{13}CH_3$, Ile-δ1-$^{13}CH_3$, Leu,Val-$^{13}CH_3$/$^{13}CH_3$, Thr-$^{13}CH_3$ and Phe, Tyr-[^{1}H,^{13}C,^{15}N] FliT$^{\Delta\alpha4}$-FliJ^{51}-101 samples were produced following a previously published protocol. (Saio et al. 2014) The sample conditions were: 20 mM sodium phosphate buffer (pH 7.0), 10 mM BME and 100 mM KCl. The labeling is referred throughout to in short form as ‘double labeled’ and ‘^{15}N-methyl/aromatic’ labeled, respectively. The protein is referred to as ‘FliT-FliJ’ in

Author Manuscript Author Manuscript Author Manuscript Author Manuscript

short form in the manuscript. A 1 mM *U*-[^{2}H,^{15}N] and Ileδ1-[^{13}CH^{3}], Leu-[^{13}CH$_3$/^{12}CD^{3}], Val-[^{13}CH$_3$/^{12}CD$_3$] ('^{15}N-methyl' in short form) maltose binding protein (MBP) sample was produced as previously described. (Gardner et al. 1998) Conditions were 20 mM sodium phosphate buffer (pH 7.0), 5 mM BME and 100 mM KCl.

NMR spectroscopy

Pulse sequence development and data collection were conducted on a Bruker Avance III 850 MHz and Bruker Avance 700 MHz spectrometers each equipped with a proton-optimized triple resonance TCI CryoProbe. Topspin 3.2 and 2.1 (Bruker BioSpin) were used for data collection on the 850 and 700 MHz spectrometers, respectively. NMRPipe (Delaglio et al. 1995) was used for spectra processing followed by analysis with NMRFAM-SPARKY. (Lee et al. 2015) Backbone, methyl and aromatic assignments for FliT-FliJ were obtained using established protocols. (Rossi et al. 2015) MBP assignments were obtained from the literature. All samples for testing were run at 32 °C. Unless specified otherwise, the NOESY mixing period was set to the standard 300 ms value in all the ^{15}N-methyl/aromatic labeled samples throughout testing.

Structure calculation and NOE analysis

Structure calculations were conducted with CYANA 3.97 automated NOESY assignment protocol (Guntert and Buchner 2015) using backbone dihedral angles (TALOS-N (Shen and Bax 2015)) and 3D-NOESY peaklists. Two datasets were prepared for CYANA that included ^{15}N and ^{13}C resolved-NOESY or their SOFAST implementations, plus, in common for the two datasets, the new SF aromatic to methyl NOESY peak list. Peak tolerances in F_1 dimension (^{1}H NOE) were set from ±0.02 ppm to ±0.01 ppm when using either the traditional or the SOFAST dataset, respectively. The ^{13}C and ^{15}N tolerances (F_2 dimension) and ^{1}H observed (F_3 dimension) remained set to ±0.1 ppm and ±0.01 ppm, respectively. NOE analysis was conducted with PdbStat v5.1. (Tejero et al. 2013)

RESULTS

Proton T_1 relaxation measurements

Proton T_1 relaxation enhancement was measured in order to evaluate the magnitude of the effect and feasibility of an L-optimized NOESY experiments in intermediate size proteins in $^{1}H_2O$. The measurements were conducted by inversion recovery at 32° C using a deuterated ^{15}N, [^{1}H,^{13}C]-Ile, [50%-^{1}H,^{13}C]-Leu and Val methyl labeled MBP (42.5 kDa) sample as detailed in Supp. Table S1. The resulting series of 1D spectra acquired with variable delay (τ) were integrated and fitted with the function:

$$I(\tau)=\mathrm{I}(0)[1-2e^{-R_z\tau}]$$

Inversion recovery experiments with both hard and selective ^{1}H pulses (Supp. Fig. S1) were run in order to extract and separate the T_1 relaxation enhancement contributions from each ^{1}H-type within the molecule and from water. The results are listed in Supp. Table S1.

Author Manuscript Author Manuscript Author Manuscript Author Manuscript

The results (Supp. Table S1) show that the amides experience a ~25% decrease in T_1 by keeping the water at equilibrium and an additional ~25% L-optimized effect by pulsing only on the amides and maintaining the sidechain magnetization at equilibrium. The effect is also present but lower in magnitude for the methyl groups where the overall drop in T_1 due to both intra and intermolecular (solvent) effects is only about 30%. With relaxation T_1 of 0.79 and 0.40 s (Supp. Table S1), the recovered magnetization [= $I(0)(1 - e^{-d1/T1})$] during interscan delay d1 of 0.2 sec is 0.22 × $I(0)$ and 0.39 × $I(0)$, respectively. The signal can be increased by 1.76× (= 0.39/0.22). The recovered magnetization during interscan delay d1 of 1.0 sec is 0.72 × $I(0)$ and 0.92 × $I(0)$, respectively. The signal can be increased by 1.28× (= 0.92/0.72). Based on these results, the use of selective pulses and HMQC-based editing in NOESY should be beneficial in achieving higher sensitivity and reduce data collection time in selectively protonated samples.

^{15}N and ^{13}C-edited 3D SOFAST-HMQC-NOESY-HMQC

The four basic variants of the 3D SOFAST HMQC-NOESY-HMQC are depicted in Fig. 1. The experiments can be subdivided into X-XH or X-YH-based experiments where the X and Y are either ^{15}N, $^{13}C_M$ or $^{13}C_{Aro}$. The X-XH-type sequences give 3D N-NH_N or 3D C_M-C_MH_M correlations Fig. 1a and 1c, respectively; the X-YH experiments give diagonal-free 3D C_M-NH_N and 3D N-C_MH_M correlations Fig. 1b and 1d, respectively. The selective pulse profiles used in this work are shown in Supp. Fig. S1. The Ernst angle optimization for these sequences is shown in Supp. Fig. S2. All the sequences presented here are listed in Supp. Table S2. All the pulse programs and parameter sets can be found in Appendix S2–S11.

In X-YH-type sequences such as in the example N-C_MH_M (Fig. 1d), a pair of shaped pulse are used immediately before the NOE mixing time in order to avoid artifacts. If only the amide flip-up shaped 90° pulse is used prior to mixing, strong artifacts are observed at the edge of the F_2 dimension. Because all pulses before NOE mixing time are acting only on amide moieties, the methyl ^{1}H signal (I_z) is not perturbed. Since that methyl (I_z) signal is observed during the second HMQC after the NOE mixing time it will appear as axial peaks in F_2 dimension. Using States-TPPI, the axial peaks are moved to the two edges of the F_2 dimension. These artifact peaks are very strong compared with pure NOE cross peaks and significantly degrade the quality of the spectrum at the edges. Different combinations of phase cycling up to 32 steps could not remove them while using a shaped pulse before mixing. Instead, two soft pulses are used, one set to at the correct $^1J_{NH}$ spacing to flip-up aromatic ^{1}H I_y to I_z, immediately following that another other one to flip-up only methyl I_z to I_y. Then the PFG during NOE mixing time dephases the methyl I_y. Therefore, the methyl ^{1}H signal before the second HMQC is suppressed and a clean spectrum is obtained.

In order to evaluate the performance of the sequences, we conducted NOE buildup experiments (Fig. 2a and Supp. Fig. S3). Integrated NOE intensities as a function of mixing time and interscan delay (d1) were collected for both SOFAST 3D and a reference WG-based 3D NOESY sequences (Kay et al. 1990) (Supp. Fig. S3a). A diagonal-free 3D ^{15}N-HMQC-NOESY-^{13}C-HMQC type-experiment that correlates N-C_MH_M and produces ‘pure’ NOE spectrum was used (Fig. 1d.). The integrated intensity from 1D experiments as a

Author Manuscript Author Manuscript Author Manuscript Author Manuscript

function of mixing time (τ) was fitted with an expression for two spins cross-correlation in the slow-motion limit (Jeener et al. 1979):

$$I(\tau)=\frac{M_0}{2}e^{-R\tau}(1-e^{-\sigma_{(H_N,H_M)}\tau})$$

where M_0 is the initial magnetization, $\sigma_{(H_N,H_M)}$ is to the *intra*-molecular cross-relaxation term between amides and methyls (MBP sample) that depends on the correlation time (τ_c) and R is the longitudinal relaxation rate at the slow-limit (Supp. Fig. S3b).

The sensitivity, or intensity scaled over the square root of total experiment time, as a function of d1 with fixed τ = 0.3 s are compared in Fig. 2b. The reference sequence (Supp. Fig. S3a) is optimized with W5 H_2O suppression (Liu et al. 1998) and flip-back pulse to remove the influence of water exchange (Stoesz et al. 1978) effects in the comparison. The results of indicate a significant benefit in sensitivity of the SOFAST-based experiment. Even at d1 = 1.0 s there is a clear advantage in using the SOFAST based sequence. Fig. 2c shows examples of excellent sensitivity gains (C_M-NH_N) and more modest ones for the C_M-C_MH_M NOESY. The sensitivities of the reference and SOFAST experiments become equal at impractically long d1 values (Fig. 2b) but the main advantage of the experiments are realized at 0.2 – 0.5 s recycle delay. The sensitivity at 0.2 s and 1.0 s are compared in Fig. 2c for the C_M-NH_N and C_M-C_MH_M 3D SOFAST HMQC-NOESY-HMQC experiments as higher and lower-level enhancement, respectively. The complete set of experiment comparison for X-XH and X-YH variants is tabulated in Fig. 2d. The results appear to follow the general trend of the measured T_1 relaxation enhancement, the methyl-methyl NOESY type experiment shows the least benefit from the SOFAST effect (Supp. Table S1).

Diagonal-free ^{13}C-aromatic to methyl 3D SOFAST-HMQC-NOESY-HMQC

The high degree of ^{13}C chemical shift separation between aromatic and methyl moieties, generally > 115ppm, makes it advantageous to restrict the acquisition window around each group in order to identify specific aromatic to methyl NOEs. For that purpose, we developed the ^{13}C-aromatic/methyl-edited 3D-SFHMQC-NOESY-HMQC. The NOE crosspeaks are acquired with high ^{13}C digital resolution and without autocorrelation and folded peaks. (Stanek et al. 2013) The pulse sequence details are given in Fig. 3a and results of the Ernst angle optimization are shown in Supp. Fig. S4. The pulse program and parameter set are displayed in Supp. Appendix S2–S11. As for all other X-YH sequences the effect of the α pulse is minimal (<5% enhancement) the reasons for that are addressed later. A schematic view of the magnetization pathway and representative ^{13}C(F_1)-^{1}H(F_3) projection of 3D spectrum for the 18.8 kDa complex between flagellar proteins FliT and FliJ are presented in (Supp. Fig. S5). The two HMQC periods before and after NOE mixing are spaced appropriately according to the aromatic and methyl proton-carbon J-couplings ($^1J_{CH}$). Previously, we had developed a reference 3D HSQC-NOESY-HMQC (unpublished work) using hard pulses and WATERGATE water suppression and compared the performance of that to the SOFAST sequence (Fig. 3a,b bottom panels). Even at d1 = 1.0 s and above the SOFAST outperforms the reference sequence by a very significant margin (last entry in Fig. 2d). This is partly due to the enhanced recovery in the SOFAST-based sequence (see ‘Fast

Author Manuscript Author Manuscript Author Manuscript Author Manuscript

pulsing in NOESY' section below) and to the more complex nature of the HSQC-based reference sequence which carries a significant S/N penalty. We were not able to achieve adequate aromatic filtering with a simpler HMQC sequence with hard ^{1}H pulses before the mixing and that alone makes the new SOFAST based sequence preferable.

One additional sequence for diagonal-free 3D $^{13}C_{Aro}/^{15}N$-edited SFHMQC-NOESY-HMQC is also available (see entry 7 in Supp. Table S2). In that pulse sequence the first SFHMQC editing is centered at the aromatic ^{13}C frequency. Following the NOESY period the magnetization is ^{15}N-edited during the second SFHMQC module. This experiment can simplify the aromatic residues assignment and can be used if the sample is labeled only on ^{15}N and aromatic moieties.

^{13}C-3D SOFAST-NOESY-HMQC

The pulse sequence diagram for ^{13}C-edited 3D SOFAST NOESY-HMQC is shown in Fig. 4a. Briefly, the selective pulses are applied to both the initial NOESY module (plus t_1 evolution), and in the SFHMQC module. Employing selective ^{1}H pulses allows for acquisition of clean sub-spectra free from aliasing at the cost of longer NOESY and t_1 evolution portion of the sequence. compared to the hard pulse version. Analogously to the aromatic-methyl experiment, selecting specific spectral windows and editing schemes allows to acquire the diagonal-free portions of the $^{1}H(F_1)$-$^{1}H(F_3)$ spectrum. In the ^{13}C-edited 3D SOFAST NOESY-HMQC the ^{1}H carrier frequency can be centered at either the amide/aromatic or the methyl position during the $^{1}H(F_1)$ frequency labeling (NOESY dimension) and two sub-spectra can be obtained, one that gives diagonal-free H_NH_{Aro}-C_MH_M-only NOEs and one that gives H_M-C_MH_M-only NOEs (see Supp. Table S2 entries 11 and 12, respectively). The pulse program and parameter set for the H_NH_{Aro}-C_MH_M and H_M-C_MH_M are displayed in Supp. Appendix S2–S11.

The resulting spectra acquired in 10 h for each SOFAST-NOESY (d1 = 200 ms) have ~1.3× higher sensitivity and ~2× higher digital resolution compared to the 'reference' 3D spectrum acquired in 50 h (d1=1.0 s) (Fig. 4b,c). High digital resolution in the indirect dimension can be reached without sparse sampling (Mobli et al. 2006) in a comparatively short time. It is worth noting that the only way to obtain such diagonal free spectrum with traditional sequences would be to use an HMQC-NOESY-HMQC scheme with ^{1}H evolution in t_1. In our testing that experiment performed very poorly compared to the SFNOESY-HMQC since the additional carbon or nitrogen HMQC evolution make the sequence longer (the lengths of a SFNOESY and a SFHMQC when t_1 is zero are 4.4 ms and 9.6 ms, respectively).

Sub-dividing the ^{1}H chemical shift window enhances the data quality and resolution particularly with high field magnets where wide frequency ranges need to be sampled. This has a tangible impact on the structure determination process (see relevant technical details in Materials and Methods section). In the case of FliT-FliJ complex peak tolerances are reduced and automated CYANA (Guntert and Buchner 2015) NOE assignment protocol yields almost twice the number of distance restraints from the SOFAST NOESY dataset vs. the reference dataset in approximately 35% of the total acquisition time (Fig. 4d).

Author Manuscript Author Manuscript Author Manuscript Author Manuscript

In addition to the experiment detailed above, similar pulse sequences were developed that utilize traditional hard proton pulses for the NOESY module in the 3D SFNOESY-HMQC sequence, in that case the ^{1}H dimension is called H_{All} (all protons in the t_1 dimension). Three separate experiments ^{15}N-only ^{13}C-only and simultaneous $^{15}N,^{13}C$-edited versions are also available (entries 12, 13, and 14 in Supp. Table S1). The experiments retain the advantages of the fast pulsing and are more suitable to double-labeled protein samples albeit without L-optimized effect. Substituting selective pulses with hard pulses in the NOESY module gives some added sensitivity in return.

Other interesting variants designed for amide/methyl labeled samples utilize the cosine modulated PC9 pulse that excites all but water protons and maintains selective pulse usage in both NOESY and HMQC modules. The sequences have H_NH_M descriptor as the t_1 frequency labeling (entries 15 and 16 in Supp. Table S1). The sequences can be either ^{13}C-edited with a carbon-only SFHMQC or simultaneously $^{15}N,^{13}C$-edited using the new simultaneous $^{15}N,^{13}C$ SFHMQC (see more description below for the new simultaneous $^{15}N,^{13}C$ SFHMQC). The first sequence gives two 3D sub-spectra while the second gives four 3D sub-spectra similarly to the $^{15}N,^{13}C$-edited 3D SOFAST-HMQC-NOESY-HMQC but with amide, and methyl ^{1}H incremented during t_1 instead of ^{15}N and ^{13}C. Lastly, if a simple PC9 pulse is utilized during NOESY, then H_NH_{Aro}-editing is achieved during t_1. Choosing ^{15}N-editing gives H_NH_{Aro}-NH_N sequences (entry 14 in Supp. Table S2). The sequence is a useful complement to the triple resonance dataset to help confirm the accuracy of backbone assignment and in favorable cases can be acquired in just a few hours. The 3D NOESY-SFHMQC can also be adapted to run on the aromatic region ($C_{Aro}H_{Aro}$-edited) and used to obtain a useful 3D H_M-$C_{Aro}H_{Aro}$ spectrum (entry 16 in Supp. Table S2).

$^{15}N,^{13}C$-edited 2D SOFAST-HMQC

A new simultaneously ^{15}N, ^{13}C-edited 2D SOFAST sequence was created for rapid titrations and for NOESY editing applications in ^{15}N, methyl labeled samples (Fig. 5a, and see entry 1 in Supp. Table S2 and Supp. Appendix S2–S11 parameters). The 2D spectrum (Fig. 5b) is acquired in ~5 minutes on an ^{15}N-methyl labeled maltose binding protein (MBP, 42 kDa) sample. This experiment slightly compromises ^{13}C sensitivity due to complications in coordinating delays Δ1 and Δ2 and different evolution times t_{1C} and t_{1N}. In addition, most of the L-optimized effect is removed since both amides and methyls are pulsed. However, it retains the Ernst angle benefit during fast pulsing (Supp. Fig. S4) and the water suppression benefit from keeping the water magnetization at equilibrium. The experiment performs better at 0.2 s d1 than either ^{15}N and ^{13}C-edited 2D HMQC with water flip-back pulses as shown in Supp. Fig. S6.

$^{15}N,^{13}C$-edited 3D SOFAST-HMQC-NOESY-HMQC

The 2D ^{15}N, ^{13}C-edited SOFAST-HMQC module is incorporated in the 3D-HMQC-NOESY-HMQC (Frenkiel et al. 1990; Zwahlen et al. 1998) experiment to give simultaneously $^{15}N,^{13}C$-edited 3D SFHMQC-NOESY-HMQC (Fig. 5c, entry 8 in Supp. Table S2 and parameters in Supp. Appendix S2–S11) in ^{15}N-selectively methyl labeled samples. The NOESY mixing period is sandwiched in between two SFHMQC pulse

Author Manuscript Author Manuscript Author Manuscript Author Manuscript

modules and a total of four 3D sub-spectra are obtained in a single experiment. In short notation, these sub-spectra are referred to as N-NH_N, C_M-NH_N, C_M-C_MH_M, and N-C_MH_M 3D-SFNOESYs, where the nucleus labels follow the acquisition order (t_1, t_2, and t_3-obs). The two mixed amide and methyl (C-N or N-C) planes are diagonal-free spectra. High quality data were obtained in only ~19h (full 3D projections are shown in Fig. 5d). The experiment was done in an effort to push the boundaries of the technique and maybe useful in sampling-limited situations as in the MBP testing sample, and only when amides and methyls are labeled. The presence of aromatics would not be optimal for carbon editing in that case.

The number of t_1 and t_2 increments depends upon the chemical shift window used for the ^{13}C and ^{15}N dimensions. In methyl/^{15}N amide labeled samples using ~35ppm in ^{15}N and ~22ppm in ^{13}C dimensions, adequate digital resolution is obtained with the current limit, that is ~118 real t_2 points (i.e. 59 complex points or 59 increments), and more points can be acquired with a smaller ^{13}C spectral width or larger ^{15}N spectral width. In t_1 dimension, the number of data points should be doubled because two sets of data acquired simultaneously.

2D Sensitivity Comparisons

Sensitivity comparison between 2D SOFAST HMQC and the 2D HSQC, HMQC and TROSY-based sequences that are currently utilized for 3D or 4D NOESY editing was conducted at fast pulsing regime (0.2 s) (Supp. Fig. S6). Comparison for relevant experiments were also conducted at 1 s and with a $^{15}N/^{13}C$-labeled protein (Supp. Fig. S7). SOFAST 2D ^{15}N and ^{13}C-HMQC experiments enhance sensitivity by 3.8× and 2.0×, respectively, compared with 2D regular HSQC experiments in H_2O. The same acquisition and processing parameters were used for these 2D experiments with a sample ^{15}N/methyl labeled MBP. Typically, relaxation delay d1, acquisition times in t_2 and t_1 dimensions were 0.2 s, 50 ms and 24 ms, respectively. The positive projections of these 2D spectra were used to compare the signal to noise (S/N). Care was taken in reporting the sensitivity results on backbone amides and accounting for differences in phases sensitive t_1 acquisition mode of TROSY vs. HMQC (Echo-AntiEcho and States-TPPI, respectively).

In the case of a uniformly $^{15}N/^{13}C$ labeled sample, the change in signal strength on the amides is more pronounced (2× from 1.6 to 3.2, Supp. Fig. S7b) because of the addition of all sidechain ^1H's enhance the T_1 relaxation (or L-optimized) effect. (Diercks et al. 2005) We anticipate the benefit of SOFAST on aliphatic groups in double labeled samples to be modest due to the fact that it is difficult to excite specific non-exchangeable side-chain moieties while leaving the rest at equilibrium.

Surprisingly, the time-shared $^{15}N,^{13}C$ 2D experiment that compromises the L-optimized effect produces good results at fast pulsing. This is in spite of the ^{13}C evolution taking a moderate sensitivity penalty. However, the sequence benefits chiefly from the use of Ernst angle pulse (Supp. Fig. S4) to enhance the signal at fast pulse.

Fast pulsing in NOESY with SOFAST-HMQC

SOFAST-HMQC leverages the flip angle (α) to increase sensitivity by increasing steady-state polarization with short recycle delay (d1 < 0.5 s). The impact of the flip angle (α) was

Author Manuscript Author Manuscript Author Manuscript Author Manuscript

carefully evaluated when applied to the 3D NOESY experiment. Supp. Fig. S2 and S4 show the flip angle (α) 1D optimizations for the six 3D SFHMQC-NOESY-HMQC variants in this work. The same principles apply to the simpler 3D NOESY-HMQC sequence with some notable difference. For the moment, we will assume that the final residual magnetization to be recycled is compatible and can be transferred to become starting magnetization in the following scan. Under these conditions, the location of the variable flip angle pulse in the 3D SFHMQC-NOESY-HMQC experiment type (Fig. 1 or Fig. 3a) should be restricted to the first ^{1}H pulse *after* the NOE mixing period. In contrast, the flip angle of the first pulse in the HMQC before mixing should be kept equal to π/2. If the flip angle is α, the signal evolution (see Supp. Appendix S1) when t_1 equals zero is:

$$I_z \xrightarrow{\alpha I_x} -I_y\sin\alpha + I_z\cos\alpha \xrightarrow{\pi I_x + \pi 2I_zS_z} -I_y\sin\alpha - I_z\cos\alpha \xrightarrow{(\pi/2)I_x} -I_z\sin\alpha + I_y\cos\alpha$$

After the flip-up π/2 pulse, a PFG is applied during the NOE mixing time, that causes the second term $I_y cos\alpha$ to be dephased and only the first term $-I_z sin\alpha$ to survive. As a result, the maximum signal can only be achieved when α of the first frequency selective ^{1}H pulse of the *first* HMQC equals π/2. Experimentally, the flip angles of the first and last pulse in the first HMQC before NOE mixing time were changed independently, and the maximum signal was obtained when both flip angles were 90°. Conversely, the flip angle of the first pulse in the *second* HMQC after NOE mixing time may be tuned for higher sensitivity at faster pulsing regime. The magnetization progresses as in the above equation with the difference that the second HMQC lacks the last π/2, and the signal is $-I_y sin\alpha - I_z cos\alpha$ before signal detection. The first term $-I_y sin\alpha$ will evolve during t_3 and the second term, $-I_z cos\alpha$, will positively contribute to the next scan if the magnetization is of the *compatible* kind. Here α is more than or equal to 90° ($\alpha \geq 90°$), therefore the $-cos\alpha$ is more than or equal to 0 ($-cos\alpha \geq 0$).

Compatible proton magnetization that can be transferred to the next scan is only present in X-XH-type experiments such as the N-NH_N 3D SFHMQC-NOESY-SFHMQC. Experiments of the X-YH-type, for example the N-C_MH_M sequence have incompatible magnetization and marginal Ernst angle effect is observed.

The following section details the distinct operating mode for the two experiment types (Fig. 1a,b and Fig. 1c,d, respectively). The spin operator analysis for the HMQC experiment is detailed in Appendix S1. Overall, the input is kI_z, and the output from the *first* HMQC is $\mp kI_z \cos(\Delta\omega_1 t_1)$ in which the ∓ sign depends on the phase setting of φ_1. During the mixing time τ, if we only consider the diagonal signal (not cross peak) the magnetization $M(\tau)$ is:

$$M(\tau) = M_0 + [M(0) - M_0]e^{-\tau R_1} \quad (2)$$

in which, M_0 is equilibrium magnetization; $M(0)$ is the initial magnetization, i.e. $M(0) = \mp k \cos(\Delta\omega_1 t_1)$; R_1 is longitudinal relaxation rate (= $1/T_1$). Resulting in:

Author Manuscript Author Manuscript Author Manuscript Author Manuscript

$$M(\tau)=M_0+[\mp k\ \cos(\Delta\omega_1 t_1) - M_0]e^{-\tau R_1} \quad (3)$$

After the *second* HMQC in 3D N-NH NOESY (or any X-XH), signal will be:

$$M(\tau)(-I_y \sin\alpha - I_z \cos\alpha) \quad (4)$$

The first term of $I_y \sin\alpha$ will be detected by the receiver. For two scans of φ_1 = (+x, −x) and φ_{rec} = (+x, −x), the detected signal will be:

$$\text{scan } i: \quad M(\tau)=M_0+[-k\ \cos(\Delta\omega_1 t_1) - M_0]e^{-\tau R_1} \quad (5)$$

$$\text{scan } i{+}1: \quad M(\tau)= -\{M_0+[+k\ \cos(\Delta\omega_1 t_1) - M_0]e^{-\tau R_1}\} \quad (6)$$

and the total detected signal by adding Eq. (5) and (6) after two scans will be proportional to $-k\cos(\Delta\omega_1 t_1)\ \sin\alpha$. The second term of $-M(\tau)I_z \cos\alpha$ is residual z component and will not be detected by the receiver, so it will not be affected by the change in receiver phase. For two scans of φ_1 = (+x, −x) and φ_{rec} = (+x, −x), the residual z component are:

$$\text{scan } i: \quad M(\tau)=M_0+[-k\ \cos(\Delta\omega_1 t_1) - M_0]e^{-\tau R_1} \quad (7)$$

$$\text{scan } i{+}1: \quad M(\tau)=M_0+[+k\ \cos(\Delta\omega_1 t_1) - M_0]e^{-\tau R_1} \quad (8)$$

and the total residual z component by adding (7) and (8) with two scans will be proportional only to:

$$-M_0(1 - e^{-\tau R_1})\cos\ \alpha \quad (9)$$

In other words, the residual z component is created from thermal recovery during the mixing time τ and the signal in the first HMQC does not contribute to the residual z component. This residual z component will be positively added to the magnetization recovered during d1 in next scan and that will be:

Author Manuscript Author Manuscript Author Manuscript Author Manuscript

$$M(d1+aq)=M_0+[M_0(1-e^{-\tau R_1})\cos\alpha-M_0]e^{-(d1+aq)R_1}=M_0(1-e^{-\tau R_1})\cos\alpha e^{-(d1+aq)R_1}+M_0[1-e^{-(d1+aq)R_1}]$$

(10)

We assume that in the very first scan of the experiment, the residual z component is supplied by the steady state scan. The signal in subsequent scan is increased because of the addition of:

$$-M_0(1-e^{-\tau R_1})\cos\alpha e^{-(d1+aq)R_1} \quad (11)$$

Please note that $\alpha \geq 90°$, and $-\cos\alpha \geq 0$. At longer τ and shorter d1, the first term in Eq 10 (or Ernst-angle contribution to signal) is more significant (see Supp. Fig. S2).

The contribution that starts at about 20% boost in signal, will vanish at longer d1 and the optimal α will become 90°.

In the N-CH NOESY (or any X-YH), the *second* ^{1}H-^{13}C HMQC does not affect the ^1H_N's magnetization from thermal recovery during τ at all. Therefore the total recovery time for the ^1H_N's magnetization is τ + aq + d1 instead of aq + d1 in a regular NOESY experiment using hard pulse. The recovered ^1H_N magnetization will be:

$$M_0[1-e^{-(\tau+d1+aq)R_1}] \quad (12)$$

When τ, aq and d1 are 0.3, 0.08 and 0.2 sec, the signal strength is increased by ~40% (see the effect of this term on the spectrum in Supp. Fig. S8).

The conclusions from the analysis are that the Ernst angle dependent term $M_0(1-e^{-\tau R1}\cos\alpha$ contributes to the higher steady state magnetization in the X-XH type experiments while the term $M_0[1-e^{-(\tau+d1+aq)R1}]$ contributes to the enhancement in the X-YH type experiments with a negligibly small contribution from the α pulse (<5%).

In the simpler 3D NOESY-HMQC of X-YH-type, both 'X' and 'Y' types ^{1}H magnetization benefit from an overall τ + aq + d1 recovery period. Taking the H_N-C_MH_M 3D NOESY-HMQC as an example, starting from the flip-up H_N pulse and ending to the first selective pulse in the subsequent scan (Fig. 4a), the H_N magnetization is not operated upon and has time to recover to equilibrium. Analogously, starting from acquisition time and ending on the flip-down pulse after τ in the following scan, the H_M magnetization is left unperturbed and has aq + d1 + (t1) + τ to recover until it is pulsed again. Here, contrary to the 3D HMQC-NOESY-HMQC, there seem to be no significant issues with axial peaks artifacts so there is no need to apply a selective pulse to flip-up the proton magnetization of the HMQC step.

Author Manuscript Author Manuscript Author Manuscript Author Manuscript

We believe that the above section accounts for most our experimental findings but we do not exclude that depending upon the specific experiment the effects may combine in a way that is not trivial to elucidate at this time.

DISCUSSION

Longitudinal relaxation optimization (L-opt) is achieved in proteins by selective excitation of a subgroup of spins leaving the surrounding population of intramolecular spins at equilibrium. (Pervushin et al. 2002) Such unperturbed spins syphon the magnetization from the excited spins allowing for faster recovery to equilibrium state. The observed effect is a decrease in proton T_1 and concomitant increase in sensitivity.

Practically, it is very straight forward to achieve significant L-opt effect on amides in small doubly labeled proteins. The amides ^{1}H's are almost completely separate from the sidechain atoms (minus the overlapping aromatics). Conversely, even with relatively narrow ~4ppm PC9 pulses it is difficult to selectively pulse on specific types of ^{13}C-bound protons (for example methyls) without perturbing a large number of surrounding spins and therefore the L-optimized effect is not very significant on the ^{13}C-bound protons. In the case of ^{2}H methyl labeled sample made with fresh $^{2}H_2O$ to insure minimal spurious protonation (< 3%) it should be possible to selectively pulse 'mostly' methyls protons. We estimated, from integration of the 1D proton spectrum, that our protein may contain up to 5% spurious protonation due to the use of repeatedly recycled $^{2}H_2O$ during sample preparation.

Based on the proton relaxation experiments (Supp. Table S1) and the 2D comparisons we concluded that SOFAST-HMQC may be advantageous for 3D NOESY acquisitions in deuterated selectively protonated samples in $^{1}H_2O$ buffer. The SOFAST experiment is HMQC rather than HSQC-based, it adopts ^{1}H shaped pulses for excitation and refocusing and uses an optimized flip angle value (Ernst angle) 'α' to further increase signal strength by carrying residual magnetization over to the next scan during fast pulsing. (Schanda et al. 2005) The HMQC pulse sequence has fewer RF pulses than HSQC and it alleviates the signal decay from pulse imperfection. The shaped pulses excite or refocus only amide $^{1}H_N$ or methyl $^{1}H_M$ (N=amide, M=methyl) and leave H_2O peak unperturbed.

In our 2D testing (Supp. Fig. S6) the SOFAST produced the highest sensitivity at 0.2 s d1. In migrating the 2D to 3D NOESYs, we painstakingly investigated the effects of water flip-back pulses in the reference WATERGATE 2D ^{15}N and ^{13}C-HMQC spectra in order to rule out that the enhancement was simply the result of not pulsing water. The enhancement figures for the basic amide, methyl and aromatic edited 3D SOFAST HMQC-NOESY-HMQC in Fig. 2d are obtained with the same number of transients, same d1 and identical acquisition parameters. Both reference and SOFAST use States-TPPI for phase sensitive acquisition. The data show that NOE buildup curves are skewed favorably toward the SOFAST experiments (Fig. 2). The maximum gains are achieved at lower d1 value and the enhancement persists even at the normal 1s d1 delay that is used in most regular NOESY experiments for practical purposes. In high field instruments with cryoprobes and samples with concentration >0.3 mM, SOFAST-NOESY experiments can be successfully run with as

Author Manuscript Author Manuscript Author Manuscript Author Manuscript

little as 0.2 – 0.5 s relaxation delay (d1). Under these conditions, the signal from reference experiment is significantly attenuated.

The SOFAST NOESY experiments benefit from a combination of the L-optimized effect and Ernst Angle (α) optimization (Supp. Fig. S2 and S4) indicating that the residual $-I_z cos\alpha$ magnetization is carried from the preceding scan to boost sensitivity in the current scan by increasing the steady state polarization during fast pulsing. In some experiment types, SOFAST NOESY also intrinsically uses the mixing time to enhance the recovery of the proton magnetization that is not used until the next transient.

There are three types of experiments and we identified two consistent mechanisms that explain the results: 1) In NOE experiments that are starting and ending on the same moiety/atom type (X-XH), such as N-NH_N, H_N-NH_N, C_M-C_MH_M, H_M-C_MH_M (and the corresponding NOESY-HMQC versions that are ^1H incremented in t_1), the residual magnetization is positively added to the magnetization recovered during d1 to increase the overall steady state polarization. Plus, the decreases in overall T_1 facilitates recovery. Optimizing the flip angle α increases the S/N by 10–15% (Supp. Fig. S2).

2) When the experiment starts on atom type ‘X’ and ends on atom type ‘Y’ (X-YH) for example as the case of N-C_MH_M 3D HMQC-NOESY-HMQC (or C_M-NH_N, C_{Aro}-C_MH_M), the residual magnetization of H_M in N-C_MH_M is not compatible and will not add to the magnetization of H_N in the next scan. The Ernst angle effect becomes marginal and optimizing the flip angle α only increases the S/N by <5% (Supp. Fig. S2). Instead, the thermal recovery of the H_N magnetization during the mixing time τ is not affected by the second HMQC because its ^1H shaped pulses are set at the H_M frequency. As a result, the relaxation recovery time for H_N will be τ + aq + d1 (aq is acquisition time) instead of aq + d1 in a regular experiment using hard 90° pulses. When mixing time (τ), aq and d1 are 0.3, 0.08 and 0.2 sec the signal is increased by 40%. Spoiling the recovery of the ‘X’ magnetization with a flip-up pulse removes that gain as shown in Supp. Fig. S8. The effect carries to the case of X-YH-type 3D NOESY-HMQC experiments such as H_N-C_MH_M, H_M-NH_N and H_M-$C_{Aro}H_{Aro}$. Here, in the absence of artifacts, both the X and Y-type proton magnetization can have τ + aq + d1 relaxation periods since the ‘Y’ magnetization is operated upon only during the HMQC.

3) In time-shared NOE experiment such as H_NH_M-$NC_MH_NH_M$ both residual $-I_z cos\alpha$ for H_N and H_M magnetizations are positively added to their respective spin magnetization recovered during d1 and contribute to higher steady state polarization. Optimizing the flip angle α increases the S/N by ~15–20% (Supp. Fig. S4). Here the L-optimized effect is marginal since we pulse all the protons except water but there is perhaps improvement from the better water suppression achieved with selective pulses as opposed to the hard/flip-back composite pulse in the traditional sequence.

Intermediate size deuterated samples that tend to have longer longitudinal relaxation and require longer mixing for NOESY (0.2 – 0.4 s) should benefit from the new experiments. Rapid collection at ultrahigh field in H_2O is a key advantage when dealing with time

Author Manuscript Author Manuscript Author Manuscript Author Manuscript

sensitive, degradation-prone proteins which often prove to be more biologically active and interesting.

Notoriously weak experiments such as the 3D ^{15}N-resolved HMQC-NOESY-HMQC are possible even in intermediate size systems (see N-N, N-C, C-N 2D projections along H_N or H_M in Fig. 5d). These are, in fact, the most sensitive experiments of dual SOFAST-HMQC-type.

Diagonal-free editing schemes can be implemented in a very straightforward manner in both 3D NOESY-HMQC and 3D HMQC-NOESY-HMQC. Diagonal-free methyl to amide and amide to methyl versions of the experiment work extremely well and provide very important crosspeaks that are symmetric and helpful to cross validate the NOE assignment. The data acquisition can be split into smaller frequency windows to greatly enhance the resolution in the NOE dimension. The example of SOFAST aromatic-methyl NOESY pulse sequence (Fig. 3a) is simpler than the counterparts using HSQC schemes (Morshauser and Zuiderweg 1999; Stanek et al. 2013; Xia et al. 2001) (Fig. 3b) and scales well to larger methyl-aromatic labeled systems. We have successfully used the sequence to assign aromatic moieties in systems up to 35 kDa kinase domain (KD) at 10° C and at relatively low concentration (200 μM). This is a particularly powerful experiment in large systems when selective ^{1}H-^{13}C aromatic ring labeling reagents are utilized. (Lichtenecker 2014) For smaller proteins, aromatic-methyl and methyl-methyl core connectivity are extracted in a very straightforward manner in fully protonated samples.

In the 3D SFNOESY-HMQC experiment, removing the first SFHMQC transfer shortens the sequence by ~5.2ms (the lengths of a SFNOESY and a SFHMQC when t_1. is zero are 4.4 ms and 9.6 ms, respectively; length of selective pulses depends on field strength) compared to the 3D SFHMQC-NOESY-HMQC with ^{1}H(F_1) incremented during t_1 and gives the more sensitive 3D SFNOESY-HMQC experiment. Diagonal-free data with high digital resolution can therefore be acquired more efficiently. The increase in resolution and reduced data collection time have a positive influence on the quality of model-based methyl and aromatic NOE assignment. During automated run protocol in CYANA (Guntert and Buchner 2015) more extensive NOE restraint network with twice the number of restraints was obtained when using the higher resolution SOFAST-based NOESY dataset.

Presently, the possible limitations of the technique emerge when attempting to study amide, aromatic or aliphatic resonances that are too close to the water ^{1}H resonance (between ~4 and 6 ppm) and are outside the selective excitation PC9 pulse bandwidth. Additionally, the methyl-based NOESY shows a very modest improvement at 1.0 s. We anticipate that for highly deuterated proteins with protons only at methyl positions in $^{2}H_2O$ the gains in sensitivity will be limited to a small Ernst angle enhancement effect <10%. Therefore the sequences are intended for proteins in non-deuterated buffer.

CONCLUSION

A new approach to 3D NOESY spectroscopy based on fast pulsing SOFAST-HMQC technology is outlined. The experiments, intended for intermediate or large size deuterated

Author Manuscript Author Manuscript Author Manuscript Author Manuscript

and selectively methyl or aromatic labeled proteins in $^{1}H_2O$. The experiments are easily to implement and, compared to traditional hard-pulse implementations, they offer shorter collection time, with enhanced sensitivity and resolution. In most cases, even with normal 1.0 s interscan delay SOFAST NOESY outperforms the traditional experiment. We have developed a series of 3D SFNOESY experiments that cover most acquisition scenarios and labeling schemes. The results demonstrate that the approach should positively impact the field of protein structure determination by liquid state NMR.

Supplementary Material

Refer to Web version on PubMed Central for supplementary material.

Acknowledgments

The authors thank Lewis Kay, Nik Sgourakis and Yoan Monneau for helpful discussions and Tao Xie and Yajun Jiang for supplying test samples.

FUNDING SOURCES

This work is financially supported by the NIH grant AI094623 to C.G.K. and by Minnesota NMR Center (MNMR).

REFERENCES

Amero C, et al. Fast two-dimensional NMR spectroscopy of high molecular weight protein assemblies. J Am Chem Soc. 2009; 131:3448–3449. [PubMed: 19243101]

Augustyniak R, Ferrage F, Paquin R, Lequin O, Bodenhausen G. Methods to determine slow diffusion coefficients of biomolecules: applications to Engrailed 2, a partially disordered protein. J Biomol NMR. 2011; 50:209–218. [PubMed: 21603954]

Delaglio F, Grzesiek S, Vuister GW, Zhu G, Pfeifer J, Bax A. Nmrpipe - a Multidimensional Spectral Processing System Based on Unix Pipes. J Biomol NMR. 1995; 6:277–293. doi: [PubMed: 8520220]

Diercks T, Daniels M, Kaptein R. Extended flip-back schemes for sensitivity enhancement in multidimensional HSQC-type out-and-back experiments. J Biomol NMR. 2005; 33:243–259. [PubMed: 16341753]

Frenkiel T, Bauer C, Carr MD, Birdsall B, Feeney J. Hmqc-Noesy-Hmqc, a 3-Dimensional Nmr Experiment Which Allows Detection of Nuclear Overhauser Effects between Protons with Overlapping Signals. J Magn Reson. 1990; 90:420–425. doi:

Gardner KH, Zhang XC, Gehring K, Kay LE. Solution NMR studies of a 42 KDa Escherichia coli maltose binding protein beta-cyclodextrin complex: Chemical shift assignments and analysis. J Am Chem Soc. 1998; 120:11738–11748. doi:

Geen H, Freeman R. Band-Selective Radiofrequency Pulses. J Magn Reson. 1991; 93:93–141. doi:

Gelis I, et al. Structural basis for signal-sequence recognition by the translocase motor SecA as determined by NMR. Cell. 2007; 131:756–769. [PubMed: 18022369]

Guntert P, Buchner L. Combined automated NOE assignment and structure calculation with CYANA. J Biomol NMR. 2015; 62:453–471. [PubMed: 25801209]

Hwang TL, van Zijl PCM, Garwood M. Broadband adiabatic refocusing without phase distortion. J Magn Reson. 1997; 124:250–254. doi: [PubMed: 9169217]

Jeener J, Meier BH, Bachmann P, Ernst RR. Investigation of Exchange Processes by 2-Dimensional Nmr-Spectroscopy. J Chem Phys. 1979; 71:4546–4553. doi:

Kay LE, Clore GM, Bax A, Gronenborn AM. 4-Dimensional Heteronuclear Triple-Resonance Nmr-Spectroscopy of Interleukin-1-Beta in Solution. Science. 1990; 249:411–414. doi: [PubMed: 2377896]

Author Manuscript Author Manuscript Author Manuscript Author Manuscript

Lee W, Tonelli M, Markley JL. NMRFAM-SPARKY: enhanced software for biomolecular. NMR spectroscopy Bioinformatics. 2015; 31:1325–1327. [PubMed: 25505092]

Lichtenecker RJ. Synthesis of aromatic C-13/H-2-alpha-ketoacid precursors to be used in selective phenylalanine and tyrosine protein labelling. Org Biomol Chem. 2014; 12:7551–7560. [PubMed: 25136818]

Liu ML, Mao XA, Ye CH, Huang H, Nicholson JK, Lindon JC. Improved WATERGATE pulse sequences for solvent suppression in NMR spectroscopy. J Magn Reson. 1998; 132:125–129. doi:

Mobli M, Stern AS, Hoch JC. Spectral reconstruction methods in fast NMR: Reduced dimensionality, random sampling and maximum entropy. J Magn Reson. 2006; 182:96–105. [PubMed: 16815055]

Morshauser RC, Zuiderweg ERP. High-resolution four-dimensional HMQC-NOESY-HSQC spectroscopy. J Magn Reson. 1999; 139:232–239. doi: [PubMed: 10423360]

Pervushin K, Vogeli B, Eletsky A. Longitudinal (1)H relaxation optimization in TROSY NMR spectroscopy. J Am Chem Soc. 2002; 124:12898–12902. [PubMed: 12392438]

Rossi P, et al. A hybrid NMR/SAXS-based approach for discriminating oligomeric protein interfaces using Rosetta. Proteins. 2015; 83:309–317. [PubMed: 25388768]

Saio T, Guan X, Rossi P, Economou A, Kalodimos CG. Structural Basis for Protein Antiaggregation Activity of the Trigger Factor Chaperone. Science. 2014; 344:597-+. doi:ARTN 125049410.1126/science.1250494.

Sathyamoorthy B, Lee J, Kimsey I, Ganser LR, Al-Hashimi H. Development and application of aromatic [(13)C, (1)H] SOFAST-HMQC NMR experiment for nucleic acids. J Biomol NMR. 2014; 60:77–83. [PubMed: 25186910]

Schanda P, Forge V, Brutscher B. HET-SOFAST NMR for fast detection of structural compactness and heterogeneity along polypeptide chains. Magn Reson Chem. 2006a; 44(Spec No):S177–S184. [PubMed: 16823898]

Schanda P, Kupce E, Brutscher B. SOFAST-HMQC experiments for recording two-dimensional heteronuclear correlation spectra of proteins within a few seconds. J Biomol NMR. 2005; 33:199–211. [PubMed: 16341750]

Schanda P, Van Melckebeke H, Brutscher B. Speeding up three-dimensional protein NMR experiments to a few minutes. J Am Chem Soc. 2006b; 128:9042–9043. [PubMed: 16834371]

Shen Y, Bax A. Protein Structural Information Derived from NMR Chemical Shift with the Neural Network Program TALOS-N. Methods Mol Biol. 2015; 1260:17–32. [PubMed: 25502373]

Solyom Z, Schwarten M, Geist L, Konrat R, Willbold D, Brutscher B. BEST-TROSY experiments for time-efficient sequential resonance assignment of large disordered proteins. J Biomol NMR. 2013; 55:311–321. [PubMed: 23435576]

Sprangers R, Kay LE. Probing supramolecular structure from measurement of methyl H-1-C-13 residual dipolar couplings. J Am Chem Soc. 2007; 129:12668-+. [PubMed: 17910459]

Stanek J, Nowakowski M, Saxena S, Ruszczynska-Bartnik K, Ejchart A, Kozminski W. Selective diagonal-free C-13,C-13-edited aliphatic-aromatic NOESY experiment with non-uniform sampling. J Biomol NMR. 2013; 56:217–226. [PubMed: 23657844]

Stoesz JD, Redfield AG, Malinowski D. Cross Relaxation and Spin Diffusion Effects on Proton Nmr of Biopolymers in H2o - Solvent Saturation and Chemical Exchange in Superoxide-Dismutase. Febs Lett. 1978; 91:320–324. doi: [PubMed: 680139]

Tejero R, Snyder D, Mao BC, Aramini JM, Montelione GT. PDBStat: a universal restraint converter and restraint analysis software package for protein NMR. J Biomol NMR. 2013; 56:337–351. [PubMed: 23897031]

Theillet FX, Rose HM, Liokatis S, Binolfi A, Thongwichian R, Stuiver M, Selenko P. Site-specific NMR mapping and time-resolved monitoring of serine and threonine phosphorylation in reconstituted kinase reactions and mammalian cell extracts. Nat Protoc. 2013; 8:1416–1432. [PubMed: 23807285]

Tugarinov V, Hwang PM, Ollerenshaw JE, Kay LE. Cross-correlated relaxation enhanced H-1-C-13 NMR spectroscopy of methyl groups in very high molecular weight proteins and protein complexes. J Am Chem Soc. 2003; 125:10420–10428. [PubMed: 12926967]

Author Manuscript Author Manuscript Author Manuscript Author Manuscript

Vuister GW, Clore GM, Gronenborn AM, Powers R, Garrett DS, Tschudin R, Bax A. Increased Resolution and Improved Spectral Quality in 4-Dimensional C-13/C-13-Separated Hmqc-Noesy-Hmqc Spectra Using Pulsed-Field Gradients. J Magn Reson Ser B. 1993; 101:210–213. doi:

Xia YL, Man D, Zhu G. 3D H-aro-NOESY-CH3NH and C-aro-NOESY-CH3NH experiments for double labeled proteins. J Biomol NMR. 2001; 19:355–360. doi: [PubMed: 11370781]

Zwahlen C, Gardner KH, Sarma SP, Horita DA, Byrd RA, Kay LE. An NMR experiment for measuring methyl-methyl NOEs in C-13-labeled proteins with high resolution. J Am Chem Soc. 1998; 120:7617–7625. doi:

Author Manuscript
Author Manuscript
Author Manuscript
Author Manuscript

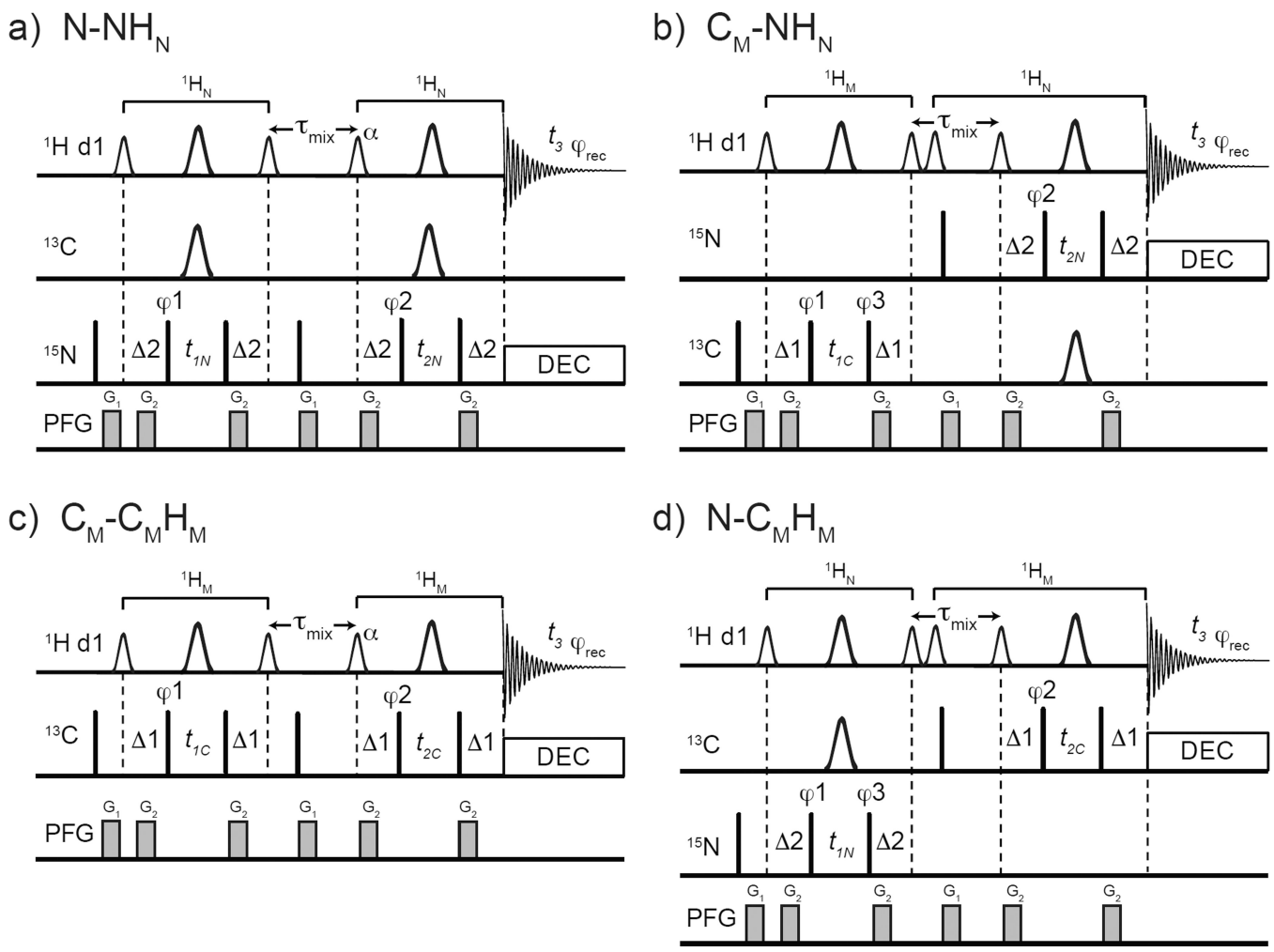

Fig. 1.

Pulse sequences for 3D SOFAST HMQC-NOESY-HMQC with the following frequency labeling combinations: a) $N(F_1)$-$N(F_2)H_N(F_3)$, b) $C_M(F_1)$-$N(F_2)H_N(F_3)$, c) $C_M(F_1)$-$C_M(F_2)H_M(F_3)$, and d) $N(F_1)$-$C_M(F_2)H_M(F_3)$. The smaller and larger ^{1}H shaped pulses are 1.69 ms long 90° PC9_4_90 (Smith 2001) and 1.15 ms long 180° REBURP (Geen and Freeman 1991), respectively. The flip angle α (110° to 90°, depending on the value of d1 and the experiment type) of the shaped pulse after τ_{mix} should be optimized (see text). Depending on the sequence, the offsets of the ^{1}H shaped pulses are −3,230 Hz (at 0.9 ppm) for methyl type pulses and 3,230 Hz (at 8.5 ppm) for amides. The narrow bars represent 90° hard pulses. The shaped pulse on ^{13}C channel represents a 500 μs long 180° smoothed CHIRP. (Hwang et al. 1997) The spectral centers of ^{15}N, ^{13}C, and ^{1}H dimensions are at 118.0, 16.5, and 4.7 ppm, respectively. The delays are: d1 = 0.2 sec, $\Delta1 = 1/(2\times{}^1J_{CH3}) = 4.0$ ms, $\Delta2 = 1/(2\times{}^1J_{NH}) = 5.2$ ms $\tau_{mix} = 0.3$ sec. The phase cycling for X-XH-type are $\varphi1$ = (x, −x), $\varphi2$ = (x, −x, −x, x), φ_{rec} = (x, −x, −x, x) and for X-YH-type are $\varphi1$ = (x, −x), $\varphi2$ = (x, −x, −x, x), $\varphi3$ = 4(x), 4(−x), φ_{rec} = (x, −x, −x, x, −x, x, x, −x). Bruker decoupling scheme bi_garp_2pl is used. The quadrature detections in *t*1 and *t*2 dimensions are acquired via States-TPPI of $\varphi1$ and $\varphi2$, respectively. The durations and strengths of the gradients are G1 = (1 ms, 15 G/cm), G2 = (1 ms, 5 G/cm).

Author Manuscript Author Manuscript Author Manuscript Author Manuscript

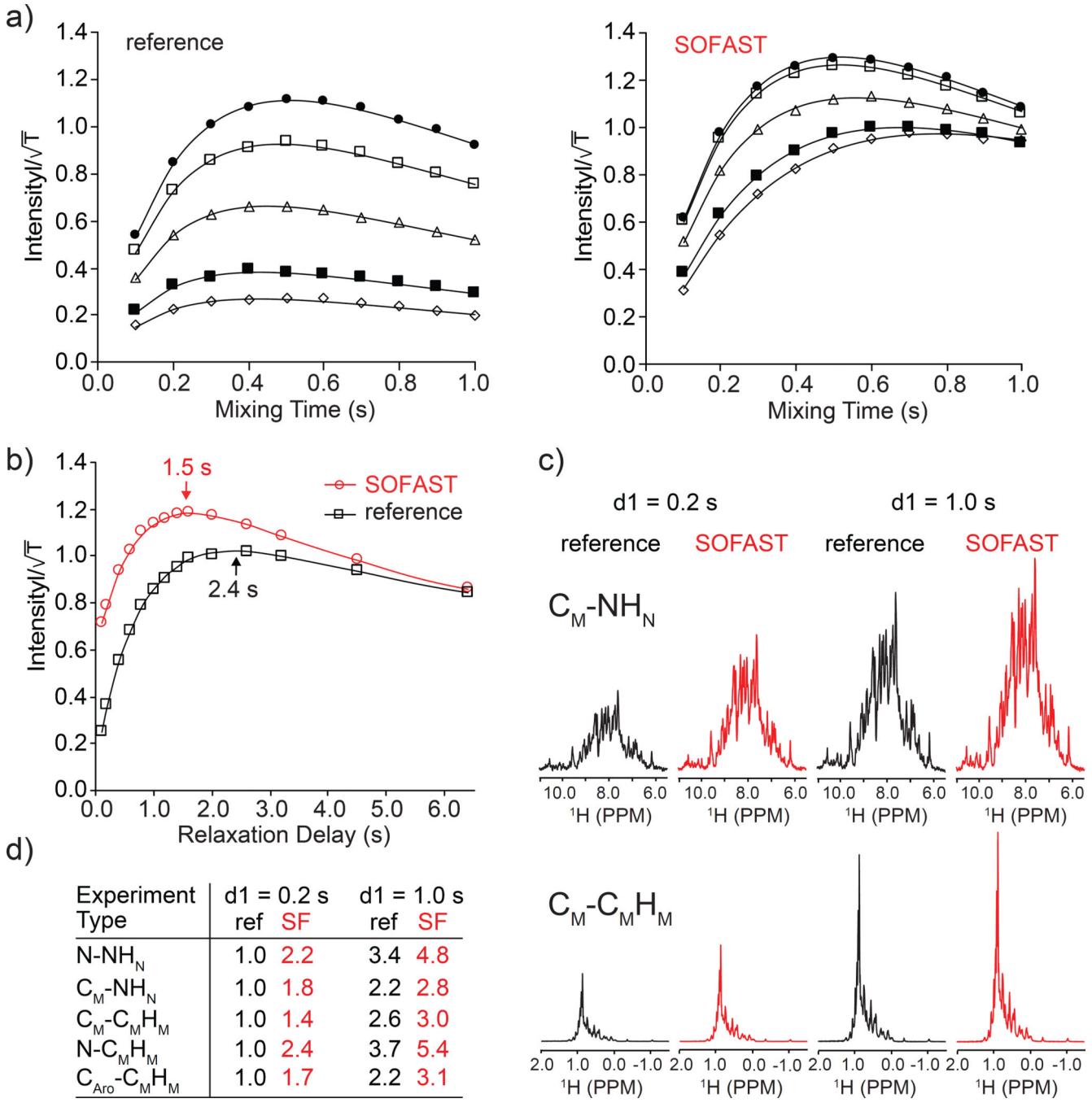

d)

Experiment Type	d1 = 0.2 s ref	d1 = 0.2 s SF	d1 = 1.0 s ref	d1 = 1.0 s SF
N-NH_N	1.0	2.2	3.4	4.8
C_M-NH_N	1.0	1.8	2.2	2.8
C_M-C_MH_M	1.0	1.4	2.6	3.0
N-C_MH_M	1.0	2.4	3.7	5.4
C_{Aro}-C_MH_M	1.0	1.7	2.2	3.1

Fig. 2.

Comparisons of NOE buildup and sensitivity for MBP U-^{15}N, [^{1}H,^{13}C]-methyl labeled sample. NOE buildup curves (a): $\mathrm{Intensity}/\sqrt{T}$ vs. mixing time where T is total experiment time were plotted at five different d1 values: 0.1 (open diamonds), 0.2 (filled squares), 0.5 (open triangles), 1.0 (open squares) and 2.0 s (filled circles). Sensitivity curves (b): $\mathrm{Intensity}/\sqrt{T}$ vs. recycle delay (d1). The first 1D spectra of diagonal-free 3D HMQC-NOESY-HMQC (N-C_MH_M) experiments used here for reference and for SOFAST are shown in Fig. 1c and Supp. Fig. S3a, respectively. The series of 1D experiments that give

Author Manuscript Author Manuscript Author Manuscript Author Manuscript

pure NOE intensity were acquired with 32 scans. The first 1D spectra used for intensity comparisons are shown for C_M-NH_N and C_M-C_MH_M (c). Tabulated intensity comparison for 3D HMQC-NOESY-HMQC sequences (d). Recycle delays 0.2 and 1.0 sec were used in (c) and (d) for reference and SOFAST versions.

Author Manuscript Author Manuscript Author Manuscript Author Manuscript

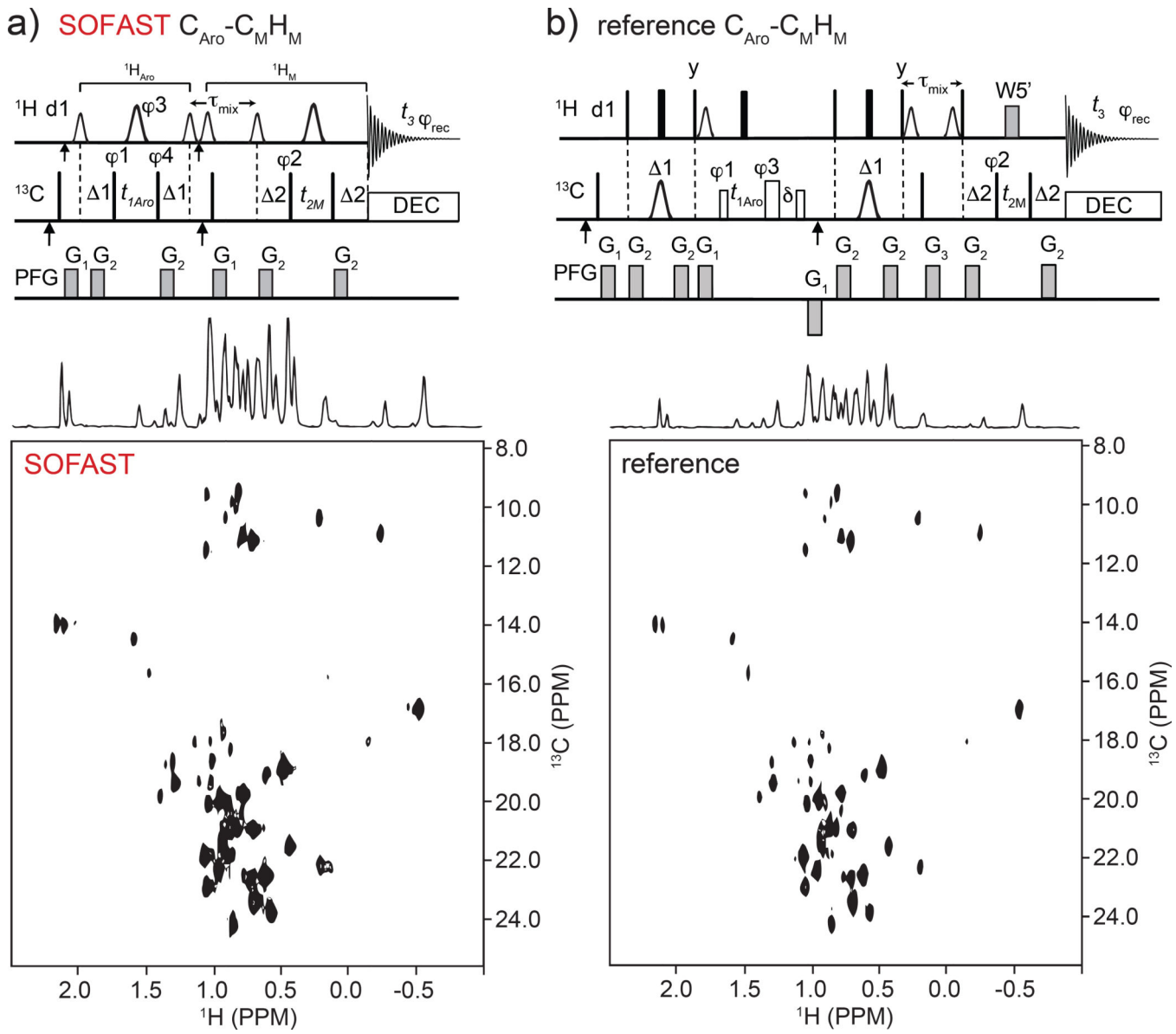

Fig. 3.

Pulse sequences in top panels are for diagonal-free Aro-Methyl 3D SOFAST HMQC-NOESY-HMQC (a) and reference 3D HSQC-NOESY-HMQC sequence (b). Frequency labeling is $C_{Aro}(F_1)$-$C_M(F_2)H_M(F_3)$. Top a): the smaller and larger ^{1}H shaped pulses are 1.69 ms long 90° PC9_4_90 and 1.15 ms long 180° REBURP, respectively. The first and second vertical arrows on ^{1}H and ^{13}C channels indicate the ^{1}H(^{13}C) carrier frequency setting to 8.5 ppm (122 ppm) and 4.7 ppm (17.5 ppm), respectively. The offsets of ^{1}H shaped pulses before and after τ_{mix} are 0 (at 4.7 ppm) and −3,230 Hz (at 0.9 ppm), respectively. The narrow bars represent 90° hard pulses. The spectral centers of $^{13}C(F_1)$, $^{13}C(F_2)$, $^1H(F_3)$ dimensions are at 122.0, 16.5, and 4.7 ppm, respectively. The delays are: d1 = 200 ms, Δ1 = 3.1 ms, Δ2 = 4.0 ms, τ_{mix} = 300 ms. The phase cycling are: φ1 = (x, −x), φ2 = (x, −x, −x, x), φ3 = 4(x), 4(y), φ4 = 8(x), 8(−x), φ_{rec} = (x, −x, −x, x, −x, x, x, −x, −x, x, x, −x, x, −x, −x, x). Bruker decoupling scheme bi_garp_2pl is used. The quadrature detections in t_1 and t_2

Author Manuscript Author Manuscript Author Manuscript Author Manuscript

dimensions are acquired via States-TPPI of φ1 and φ2, respectively. The durations and strengths of the gradients are G1 = (1 ms, 15 G/cm), G2 = (1 ms, 5 G/cm). Top (b): reference WATERGATE (W5') 3D HSQC-NOESY-HMQC pulse sequence used for the S/N comparison. The filled narrow and wide bars represent 90° and 180° hard pulses, respectively. The open narrow (41.6 μs) and wide (37.2 μs) bars on ^{13}C channel represent 90° and 180° soft pulses, respectively, that have null excitation at an offset of 109 ppm. ^{13}C shaped pulses are 423 μs IBURP2.1000 180° pulses (Geen and Freeman 1991). The first and second vertical arrows indicate the 13C carrier frequency setting to 122.0 ppm and 17.5 ppm (centers of aromatic and methyl ^{13}C chemical shifts), respectively. The distances between 3-9-19 W5' pulses are 148 μs. The delays are: d1=1.0 sec, Δ1 = 3.1 ms, Δ2 = 4.0 ms, δ = $t_1(0)$ + 2*pw (initial t_1 value and ^{1}H 180° pulse width), τ_{mix} = 0.3 sec. The phase cycling is: φ1 = (x, −x, −x, x), φ2 = (x, −x), φ3 = 4(x), 4(y), φ_{rec} = (x, −x, −x, x, −x, x, x, −x). Bruker decoupling scheme bi_garp_2pl is used. The quadrature detections in *t*1 and *t*2 dimensions are acquired via States-TPPI of φ1 and φ2, respectively. The durations and strengths of the gradients are G1 = (1 ms, 10 G/cm), G2 = (1 ms, 5 G/cm), G3 = (2 ms, 10 G/cm). Bottom panels show comparison of pure NOE F2(C_M)-F3(H_M) planes run using the FliT-FliJ complex sample (see main text Materials and Methods) that contained both ^{1}H-^{13}C methyl and aromatic labels. Mixing time was 0.3 s, d1 = 0.2 s, and 90 degrees variable angle pulse (α) for SOFAST version.

Author Manuscript Author Manuscript Author Manuscript Author Manuscript

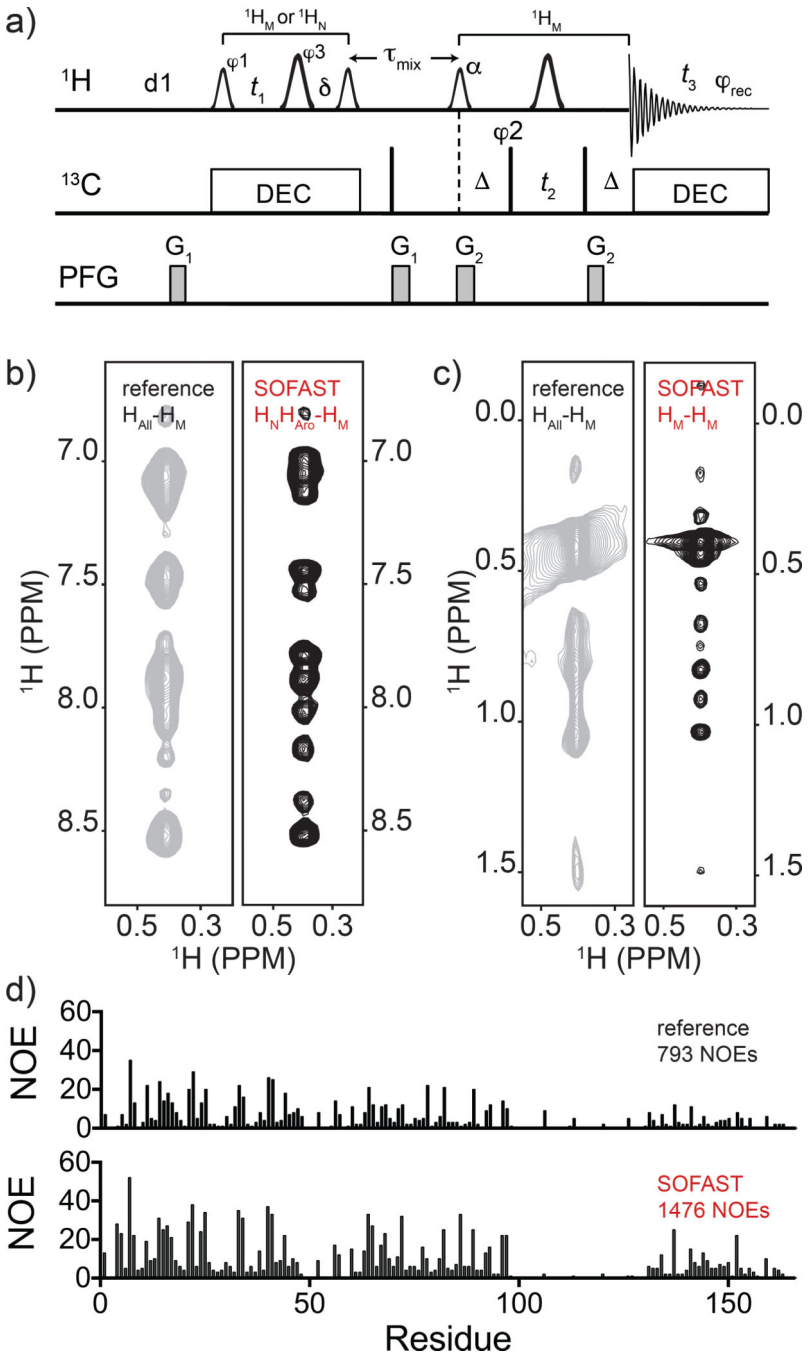

Fig. 4.

Panel a): pulse sequence of ^{13}C-edited 3D SFNOESY-HMQC for frequency labeling $H_M(F_1)$-$C_M(F_2)H_M(F_3)$ or $H_{N,Aro}$-C_MH_M (with addition of two ^{15}N 180° hard pulses at the t_1 and δ midpoint). The smaller and larger ^{1}H shaped pulses are 1.69 ms long 90° PC9_4_90 and 1.15 ms long 180° REBURP, respectively. The flip angle (α) of the shaped pulse after τ_{mix} should be optimized as discussed in maintext. The first and second vertical arrows indicate the ^{1}H carrier frequency setting to 0.9 ppm for $C_M(F_2)H_M(F_3)$ (8.5 ppm for $H_{N,Aro}$-C_MH_M) and 4.7 ppm, respectively. The offsets of ^{1}H shaped pulses before and after τ_{mix} are

Author Manuscript Author Manuscript Author Manuscript Author Manuscript

0 Hz (at 4.7 ppm) and −3,230 Hz (at 0.9 ppm), respectively. Please note that two refocusing ^{15}N 180° hard pulses at the midpoint of t_1 and δ should be added for $H_{N,Aro}$-C_MH_M. The spectral centers of ^{1}H(F_1), ^{13}C(F_2), ^{1}H(F_3) dimensions are at 1.0, (8.5 for $H_{N,Aro}$-C_MH_M), 16.5, and 4.7 ppm, respectively. The delays are: d1 = 200 ms, δ = t_1(0) + 2×pwN (initial t_1 value and ^{15}N 180° pulse width), Δ = 4.0 ms, τ_{mix} = 300 ms. The phase cycling are: φ1 = (x, −x), φ2 = (x, −x, −x, x), φ3 = 4(x), 4(y), φ_{rec} = (x, −x, −x, x, −x, x,×−x). Bruker decoupling scheme bi_garp_2pl is used. The quadrature detections in t_1 and t_2 dimensions are acquired via States-TPPI of φ1 and φ2, respectively. The durations and strengths of the gradients are G1 = (1 ms, 15 G/cm), G2 = (1 ms, 5 G/cm). Comparisons of ^{13}C-resolved 3D NOESY-HMQC with ^{13}C-resolved SFNOESY-HMQC counterpart are shown in b) and c) left and right strips, respectively. Experiments were run on ^{15}N-methyl-aromatic labeled FliT-FliJ sample and processed in an identical manner. In the reference spectrum the full 11ppm indirect ^{1}H dimension is sampled (H_{All}) while in the SOFAST sequence the acquisition is split into two 3Ds, one centered on the indirect-detected amide/aromatic (H_NH_{Aro}) (b), and one on the methyl (H_M) ^{1}H chemical shift (c). Note that the same 3D-NOESY-HMQC strip marked as ‘reference’ is split into two halves for side-by-side comparison. In (d) the number of NOE per residue (and totals) resulting from CYANA automated NOESY assignment protocol for the FliT-FliJ protein are shown for the ‘reference’ (upper) and SOFAST datasets (lower).

Author Manuscript Author Manuscript Author Manuscript Author Manuscript

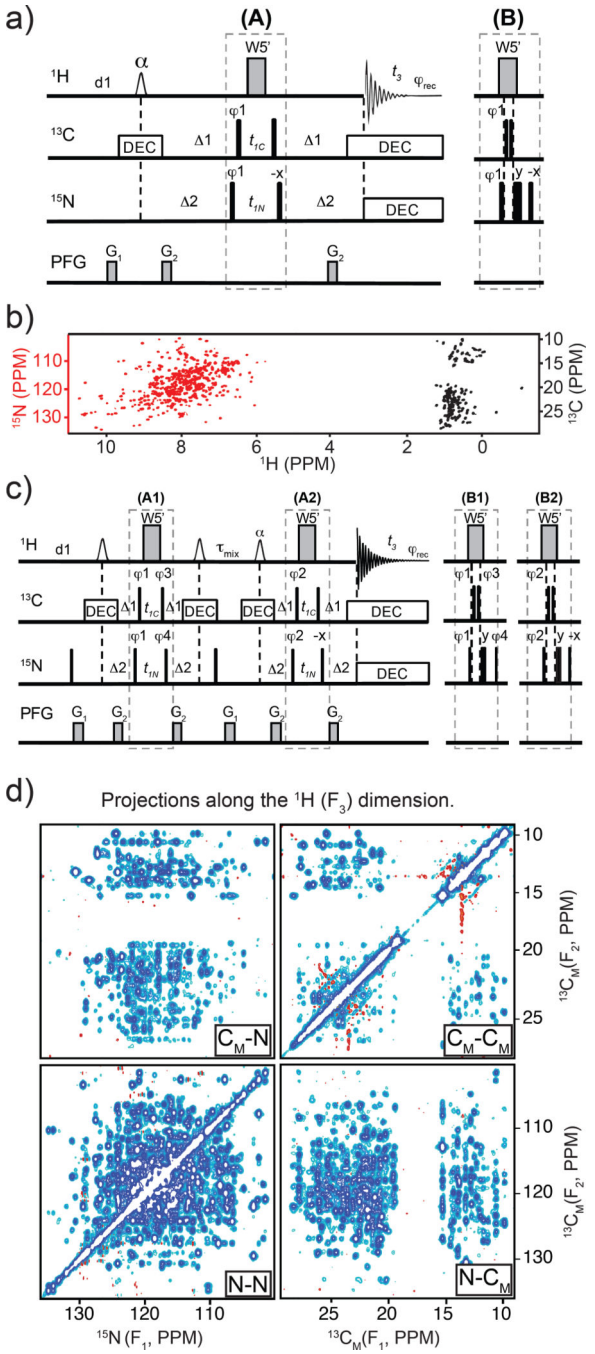

Fig. 5.

Panel a): pulse sequence diagram for simultaneous ^{15}N,^{13}C-edited 2D SFHMQC. When t1 equals to zero, the inset (B) replaces the part (A) to avoid simultaneous ^{13}C and ^{15}N hard pulses. The ^{1}H shaped pulse is a cosine-modulated PC9 pulse of 1.69 ms in length, its frequency offset is 0 Hz (at 4.7 ppm), the modulation frequency is 3,230 Hz (see detail in text). The narrow bars represent π/2 hard pulses. The distances between W5' are 148 μs. The spectral centers of $^{15}N(F_1)$, $^{13}C(F_1)$, and $^{1}H(F_2)$ dimensions are at 118.0, 17.0, and 4.7 ppm, respectively. The delays are: d1 = 200 ms, Δ1 = 4.0 ms (methyl $1/(2^{1}J_{CH})$), and Δ2 =

Author Manuscript Author Manuscript Author Manuscript Author Manuscript

5.2 ms (amide $1/(2^1J_{NH})$). The phase cycling is: $\varphi 1 = (x, -x)$, $\varphi_{rec} = (x, -x)$. Bruker decoupling scheme bi_garp_2pl is used for both ^{13}C and ^{15}N, respectively. The quadrature detection in t_1 dimension is done via States-TPPI of φ1. G1 = (1.0 ms, 15 G/cm), G2 = (0.3 ms, 10 G/cm). Panel b): 2D simultaneous ^{15}N,^{13}C-edited SFHMQC spectrum of MBP. Panel c): pulse sequence diagram for simultaneous ^{13}C,^{15}N-edited 3D SFHMQC-NOESY-HMQC. When t1 equals to zero, the inset (B1) and (B2) replace the parts (A1) and (A2), respectively, to avoid simultaneous ^{13}C and ^{15}N hard pulses. The shaped pulses, delays, pulse field gradients (PFG) and decoupling schemes are the same as those in (a). The phase cycling are: $\varphi 1 = (x, -x)$, $\varphi 2 = (x, -x, -x, x)$, $\varphi_3 = 4(x), 4(-x)$, $\varphi_4 = 4(x), 4(-x)$, $\varphi_{rec} = (x, -x, -x, x, -x, x, x, -x)$. The quadrature detections in t_1 and t_2 dimension are acquired via States-TPPI of φ1 and φ2, respectively. Two sets of two 3Ds are acquired with alternate φ4 phases (adding 0 or 180°). Addition and subtraction of the two sets result in cross-correlated ^{15}N and ^{13}C signals during t_1. Bruker AU program “split ipap 2” is used to split the two data sets. Panel d): 2D projections of simultaneously ^{15}N,^{13}C-resolved 3D SFHMQC-NOESY-HMQC run on ^{15}N-methyl labeled MBP at 32 °C. The four 2D planes are labeled as shown in the 2D axis, for example: C_M-C_M signifies $^{13}C_M(F_1)$-$^{13}C_M(F_2)$-$^1H_M(F_3)$. The third dimension of each 3D is the observed proton dimension, either the amide (^1H_N) or methyl (^1H_M).